Metal Nanoclusters for Biomedical Applications: Toward In Vivo Studies

Estelle Porret, Xavier Le Guével, Jean-Luc Coll

Metal Nanoclusters for Biomedical Applications: Toward *In Vivo* Studies

Estelle Porret, Xavier Le Guével* and Jean-Luc Coll*

Grenoble Alpes − INSERM U1209 − CNRS UMR 5309, 38000 Grenoble, France

Estelle.porret@univ-grenoble-alpes.fr
Xavier.le-guevel@univ-grenoble-alpes.fr
Jean-luc.coll@univ-grenoble-alpes.fr

Abstract

In parallel with the rapidly growing and widespread use of nanomedicine in the clinic, we are also witnessing the development of so-called theranostic agents that combine diagnostic and therapeutic properties. Among them, ultra-small gold nanoclusters (Au NCs) are showing promising potential due to their optical properties and activatable therapeutic activities under irradiation. Furthermore, due to their size smaller than 6 nm and unique biophysical properties, they also present intriguing behaviors in biological and physio-pathological environments.

In this review, we aim to present the last researches published on such nanoparticles in animals. We also propose guidelines to identify the main physico-chemical parameters that govern Au NCs behavior after administration in small animals, notably concerning their renal elimination and their ability to accumulate in tumors. Then, we present recent advances for their use as theranostic agents putting them in parallel with others contrast agents.

Keywords: Nanoclusters, gold, theranostic agent, nanomedicine, oncology, *in vivo* studies

Abbreviations

BSA : bovine serum albumin
CI : contrast index
cRGD : cyclic RGD
DTPA : diethylenetriamine penta-acetic acid
EPR : enhancement permeability and retention
FA : folic acid
FR : folate receptor
HA : hyaluronic acid
HD : hydrodynamic diameter
H : hour
ID : injected dose
ID/g : percentage of injected dose per gram of tissue
KFT : kidney filtration threshold
LA : lipoic acid
LHRH : Luteinizing hormone-releasing hormone
LIBS : laser induced breakdown spectroscopy
LMCT : ligand-to-metal charge transfer
LMMCT: ligand-t-metal-metal charge transfer
MRI : magnetic resonance imaging
NCs : nanoclusters
NIR : near-infrared
NPs : nanoparticles
PDT : photodynamic therapy
PEG : polyethylene glycol
PET : positron-emitting tomography
pi : post injection
PL: photoluminescence
PNA : peptide nucleic acid
PTT : photothermal therapy
QY : quantum yield
ROS : reactive oxygen species
RES : reticuloendothelial system
SG: glutathione
SWIR: shortwave infrared
$t_{1/2\alpha}$: distribution half-life
$t_{1/2\beta}$: elimination half-life
UV : ultraviolet
X-ray CT : X-ray computing tomography
Zw : zwitterion molecules

Table of Contents

ToC figure

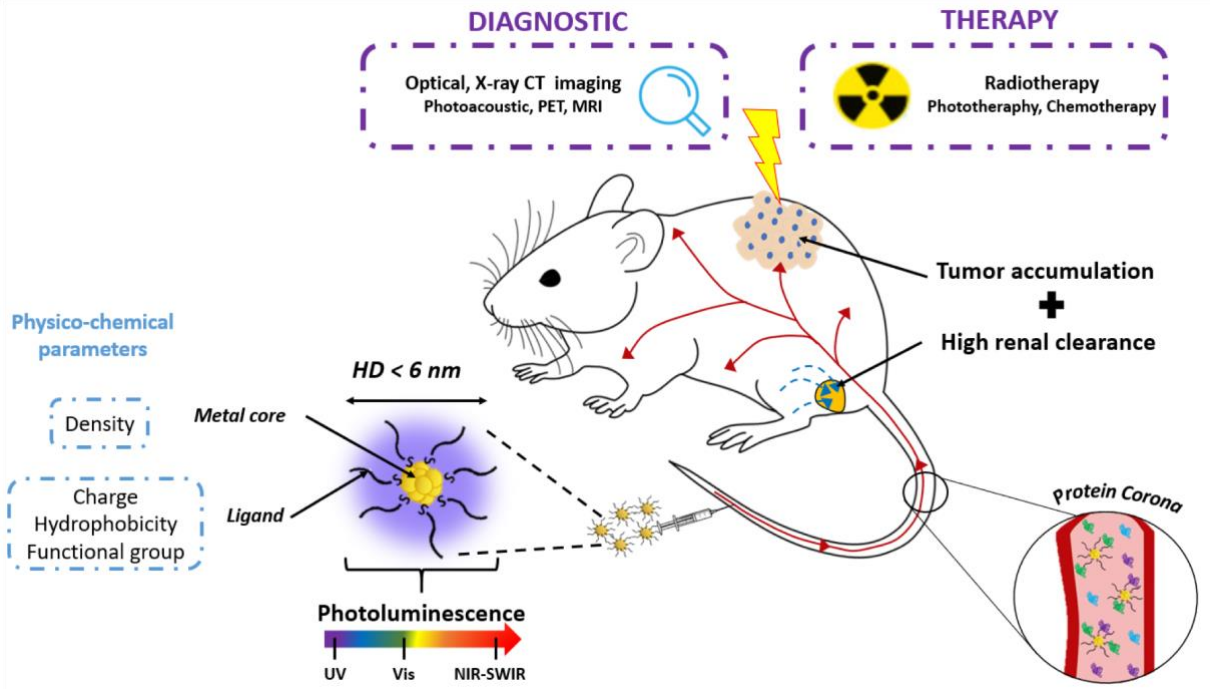

ToC Key Mord : Theranostic AuNCs

1 INTRODUCTION

In the past few years, a new class of photoluminescent ultra-small size metal **nanoparticles (NPs)** with a core size between 0.2 and 3 nm and usually referred in literature as **nanoclusters (NCs)**[1] have gained growing interest in biomedical applications. They are composed of an assembly of tens to hundreds of metallic atoms (gold, silver, platinum, zinc, copper, etc.)[2-6] stabilized by ligands (organic thiolate molecules[7-15], dendrimers[16-18], DNA[19, 20], amino acids[21-23], peptides[24-26], or proteins[27-29]). NCs can be viewed as the missing link between metal–ligand complexes and plasmonic metal NPs.

Their optical and physicochemical properties are suitable for biomedical applications since:

- Their ultra-small size should favor renal elimination, but increase passive accumulation in the tumor micro-environment compared to small molecules[30].
- They can be detected *in vivo* by multimodal imaging techniques owing to their tunable **photoluminescence (PL)**, from **ultra-violet (UV)** to **near-infrared (NIR)** region[17] and by X-ray CT[31, 32] or recently by photoacoustic imaging [33] owing to their metallic composition.
- They can be used as radio-sensitizers[34-36] due to the electronic properties of metal NCs
- They can be used as delivery systems[37-39].

Gold is often preferred over other metals for biomedical applications because of its biocompatibility and inertness. Therefore, we mainly focus this review on the *in vivo* studies of gold NCs (Au NCs).

2 Design of Au NCs

2.1 Synthesis parameters

Au NCs can be synthesized in solution by the *classical "bottom-up" approach* using metal precursors. Depending on the nature of the ligands and the synthesis parameters such as the metal : ligand : reducing agent proportion, pH, temperature, or strength of reducing agents, a large library of Au NCs have been synthesized and used for *in vivo* studies[40]. They can be divided into two main categories.

The **first one** corresponds to Au NCs with a discrete composition at the atomic level synthesized with thiolated molecules. These clusters are represented by their formula $M_n(L)_m$, where n and m are respectively the number of metal atoms (M) and ligands (L = thiolate ligand SR[31] or poly(amino-amide) PAMAM[17]).

Using this approach, it was difficult to control the growth of single-size stable Au NCs and final products was often composed of mixtures of Au NCs[24, 41]. Furthermore, it was challenging to synthesize gram-scale monodispersed Au NCs. In 2007, a so-called **etching** method was then proposed[42] based on excess ligands with increasing temperature to obtain stable and single-size Au NCs. This process, was

first used to produce $Au_{25}SG_{18}$ in large scales[43], prior to inclusion into a **size-focusing methodology** with the aim to extend the obtention of large-scale monodispersed Au NCs of other sizes such as$Au_{10}SG_{10}$, $Au_{15}SG_{13}$, $Au_{18}SR_{13}$ (SR = SG, S-*c*-C_6H_{11}), $Au_{38}SR_{24}$ and $Au_{144}SR_{60,}$(SR = SC_2H_4Ph, $SC_{12}H_{25}$)[1, 44-46]. Two recent reviews have summarized the advances in Au NC synthesis and their properties[44, 47]. Size focusing still has some limitations to obtain atomically precise Au NCs with some ligands. Au NCs stabilized with **polyethylene glycol (PEG)[15, 48], zwiterrions (Zw)**[8, 33] or proteins (**"bovine serum albumin" BSA** or transferrin)[27, 29] ligands exhibit some polydispersity and correspond to the **second category** of Au NCs: subnanometer-scaled NPs with a core size between 1 and 3 nm[49].

2.2 Specificities of the Au NCs for *in vivo* applications

2.2.1 Ultra-small size

The two main elimination pathways of NPs from the body are the urinary and hepatic systems. The first one is often preferred because it is a quick filtration process from the blood through the kidney to the bladder. More precisely, according to their different pore size, the NPs pass through the glomerular capillary walls into the endothelium (70-90 nm), the glomerular basement membrane (2-6 nm), and the podocyte (4–11 nm)[35, 45, 46]. The combined effects of these three layers have a fixed **kidney filtration threshold (KFT)** around 6-8 nm for spherical NPs (**Figure 1**)[50, 51]. Spherical metal NPs with HD below 6-8 nm, around 40 kDa[52] are thus expected to be eliminated by the kidney. NPs with a larger HD are generally retained in the RES through nonspecific uptake by specific macrophages of the liver (Kupffer cells) and the spleen due to the endothelial leakiness effect. Indeed, the liver is composed of non-continuous endothelial cells with vascular fenestration between 50 and 100 nm and the inter-endothelial cell slit of the spleen is between 200 and 500 nm**[53].** There are thus typical cut-off sizes that control the elimination and the nonspecific storage of the NPs in the body.

A study was conducted to follow the biodistribution of Au and Ag NPs with sizes ranging between 1.4 and 250 nm after intravenous administration in mice. It confirmed the size-dependent toxicity of NPs. If small NPs were widely spread into the organs, larger ones were mainly found in the liver and spleen[54]. The accumulation of metal NPs in different organs is considered as a major issue due to their poor degradation that could induce acute toxicity[53, 55].

A deeper toxicology study[56] was carried out on Au NPs with sizes between 3 and 100 nm after their intraperitoneal injection in mice. Surprisingly, the smallest and largest NPs (3, 5, 50, and 100 nm) did not show any harmful effects in mice, while those with intermediate sizes (8, 12, 17, and 37 nm) induced severe sickness that can lead to premature death in mice. These studies revealed the potential toxicity of Au NPs larger than 6 nm and advantages to use ultra-small Au NCs**.**

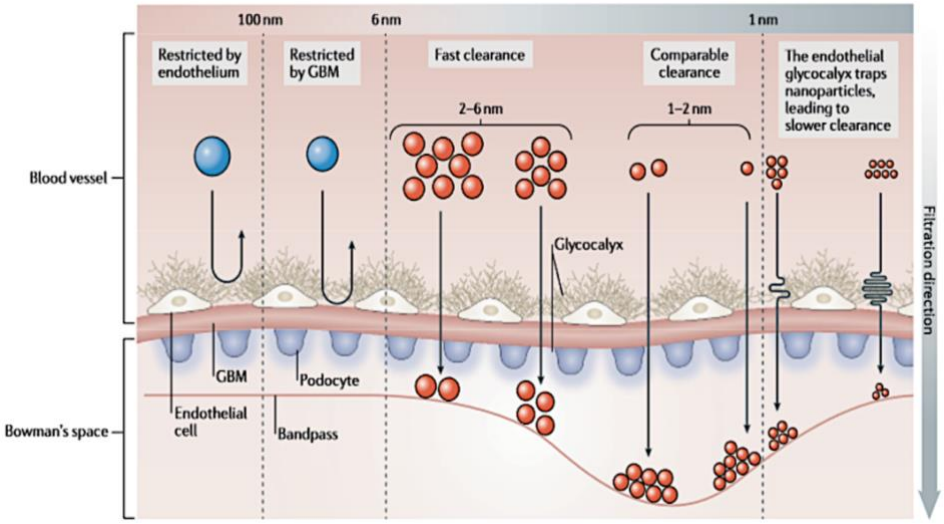

Figure 1. Layer composition of the glomerular filtration barrier.

The filtration flows through the endothelial fenestrae, across the glomerular basement membrane and the pores between podocytes. The combination of these three layers defines the size of the compounds that could cross the glomerular filtration barrier.

Reproduced from Ref [22] *with permission from Springer Nature publishing group.*

2.2.2 Optical properties

Owing to their sub-nanometer diameter, Au NCs exhibit molecular-like properties such as discrete electronic states (HOMO-LUMO, highest occupied molecular orbital and lowest unoccupied molecular orbital), leading to photoluminescence (PL) properties tunable from the UV to the NIR[17]. The PL has been attributed to complex and multiple energy transfers taking place in the metal core via **metal-to-metal charge transfer (MMCT),** and between the metal and the ligands via **ligand-to-metal charge transfer (LMCT) or ligand-to-metal-metal charge transfer (LMMCT)**. The correlation between the structure of NCs and their optical properties is still not completely understood.

Several Au NCs exhibit PL in the NIR window between 600 and 850 nm[14, 21, 57]. Very recently, the spectral window has been extended to the **shortwave infrared (SWIR)** region (900-1700 nm)[58]. Developing biocompatible optical probes in the NIR/SWIR optical window presents an advantage for *in vivo* imaging in deep tissues due to reduced auto-fluorescence, exponential decrease in light scattering and improved penetration of light into the tissues, offering potentially a higher spatial resolution[59]. Au NCs also present large Stokes shift, which can exceed 100 nm[60, 61]. This reduces the scattering and the absorption of light and improves fluorescence detection.

The main limitation of atomically precise Au NCs as optical probes is related to their low **quantum yield (QY)** especially in the NIR/SWIR windows**.** Most of the Au NCs exhibit a QY < 1% with the well-characterized $Au_{25}SG_{18}$ exhibiting a QY ~0.3%[62], which is 10^7 times higher than that of bulk gold[63].

Fortunately, few Au_nSG_m exhibit higher QYs, such as $Au_{18}SG_{14}$ ($\lambda_{exc../em..}$= 590nm/745nm, QY~5.3%)[64] or $Au_{22}SG_{18}$ ($\lambda_{exc../em..}$= 520nm/665nm, QY~8%)[65]. Different strategies have been reported to improve the brightness of Au NCs based on **i)** doping with another metal[66-68] **ii)** using ligands that can delocalize their electronical density to the gold core[69, 70], or **iii)** to rigidify the ligand shell surrounding the metal core[57, 71, 72].

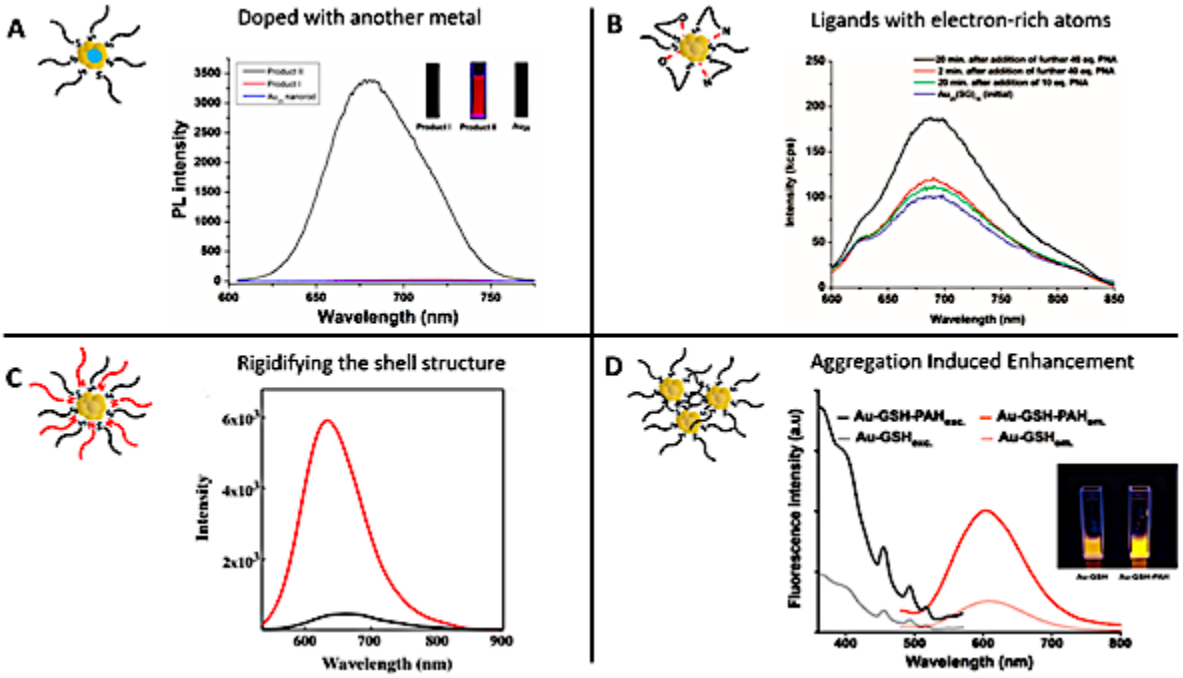

Figure 2. Strategies to enhance the PL of the metal NCs.

(A) Silver doping: Product I was obtained by reacting Au NPs with Ag^I thiolate complex, which gave rise to Ag_xAu_{25-x} NCs with a maximum of 12 Ag atoms. Product II was obtained by reacting Au_{11} NCs with Ag^I thiolate complex, which gave rise to $Ag_{13}Au_{12}$ NCs. The PL spectra of Au_{25} NCs (bottom, blue line), Product I (middle, red line), and Product II (top, black line) show that the number of silver atoms has a strong impact on the optical properties of the NCs. The inset presents the fluorescence emission of the solution of the corresponding products under UV illumination ($\lambda_{exc.}$ = 365 nm).

(B) LMCT: Luminescence spectra of $Au_{25}SG_{18}$ (blue) and after the addition of different equivalents of an electron-rich atom, PNA (initial concentration of $Au_{25}SG_{18}$: 1.1 μM, OD_{614}~0.025, $\lambda_{exc.}$ = 514 nm).

(C) Rigidification of the shell: Luminescence spectra of the $Au_{22}SG_{18}$ (black) and after the addition of tetraoctylammonium cations (red) into toluene to rigidify the shell of ligands (OD_{514}~0.025, $\lambda_{exc.}$ = 514 nm).

(D) AIE effect: Excitation and emission spectra at similar Au NC concentrations of AuSG (dashed lines) and after the addition of PAH to promote electrostatic cross-linking between Au NCs (PAH-AuSG, solid lines). The inset presents the fluorescence emission of the solution of the corresponding products under UV illumination ($\lambda_{exc.}$ = 366 nm).

Reproduced with permission from John Wiley and Sons for (A) Ref. [36a]*, and American Chemical Society for (B) Ref.* [37]*, (C) Ref.* [38a]*, and (D) Ref.* [41]

Therefore, it is crucial to develop new strategies to improve their QY. One **first approach** to enhance the brightness involves **doping Au NCs with another metal.** As an example, Rongchao Jin *et al*. obtained a QY around 40% by doping Au NCs with 13 silver atoms[66] (**Figure 2A**). We also obtained a QY around 15% by doping AuSG with silver[67]. Similar results were obtained when doping Au NCs with 2% of different metals (Ag, Cu, Pt, Zn, and Cd).[68]A **second approach** is based on the use **of ligands that can delocalize their electronical density** to the gold core. By replacing hexyle (C_6H_{13}) by dodecyle ($C_{12}H_{25}$) to stabilized the Au_{25}, or by mixing $Au_{25}SG_{18}$ with a **peptide nucleic acid (PNA)** containing electron-rich atoms (e.g. O, N) induced a 2-3 fold enhancement of the PL[69] (**figure 2B**). The exchange of some ligands of the $Au_{38}(SPhC_2)_{24}$ by $HSPhNO_2$ rather $SPhOCH_3$ also induced en increased of the PL[70]. A **third strategy is based on blocking the loss of energy** caused by intramolecular rotation of the ligand, by rigidifying the shell structure. Very bright fluorescent $Au_{22}SG_{18}$ (QY~62% in toluene, $\lambda_{em.}$ = 630 nm) were obtained after adding tetraoctylammonium cations while the initial NCs presented a QY~7% (in water, λ_{em} = 665 nm)[71] (**Figure 2C)**. A rigidification of the shell structure of Au NCs stabilized **with 6-aza-2thiothymine (ATT)** was also obtained by adding L-arginine (QY~65%, versus QY~1.8% for the NCs alone; $\lambda_{em.}$ = 530 nm)[72]. It is also possible to rigidify the shell by creating a second layer and a PL enhancement of 300 was observed when the ratio Au : Zw passed from 1 : 1 to 1 : 40[57].

Finally, the **aggregation-induced enhancement effect*[73]*** can also be seen as an elegant strategy to boost Au NCs PL. Indeed, aggregation will create stronger intra- and inter-complex aurophilic Au(I)---Au(I) interactions that could enhance the PL signal. At the same time, the intramolecular rotation and vibration of the ligands are reduced and the Au core are better protected from solvent molecules., thereby reducing the probability of nonradiative relaxation of the excited states[47, 74]. These two phenomena induce an enhancement of the emission of the NCs. By generating self-assembled AuSG using cationic polyelectrolytes such as **poly(allylamine hydrochloride) (PAH),** it was possible to control the distance between Au NCs by adjusting the pH and to increase the QY from 7 to almost 25% using AIE effect[75] (**Figure 2D**).

2.2.3 Surface properties

Surface functionalization of Au NCs has been largely investigated and an extensive library of biocompatible ligands able to generate either **electrostatic repulsion** such as small organic molecules[7-11], amino acids[21, 22], and peptides[24-26] and/or **steric repulsion** such as proteins[27-29], DNA[19, 20], dendrimers[16-18], between NCs have been used.

For example, zwitterions based on **lipoic acid sulfobetaine (LA-sulfobetaine)**, a bidentate thiol ligand with strong anchors to the metal surface, present remarkable colloidal stability in various media with high antifouling effects[8, 13, 76], while pegylated ligands are often used as a biocompatible capping agent to form a hydrating layer and generate steric hindrance between the NCs[8, 13-15].

Other small organic molecules and biomolecules are also commonly used for functionalizing the NC surface:

- fluorophores to shift the optical properties of Au NCs toward the NIR region[23, 77, 78]; drugs, photo, or radiosensitizers for cancer therapy;
- targeting molecules to specifically interact with receptors overexpressed at the surface of tumor cells, such as:
    - **Folic acid (FA)** that can recognize the folate receptors (FRs), overexpressed in many human cancer cells (ovary, breast, colon, kidney, liver, testes, brain, lung, and blood)[78-82],
    - **Luteinizing hormone-releasing hormone (LHRH)** overexpressed in several types of cancer cells (ovary, breast, prostate, lung, and liver)[83],
    - **Hyaluronic acid (HA)** that can bind to CD44 receptors overexpressed at the surface of different cancer cells, in particular cancer stem cells[80],
    - AMD3100 that can interact with CXCR4, an up-regulating receptor, in particular in leukemia or breast cancer cells[84],
    - **Cyclic RGD (cRGD)**, a zwitterionic compound capable of interacting with $\alpha_v\beta_3$, $\alpha_5\beta_1$, and $\alpha_v\beta_5$ integrins highly present in neoangiogenic endothelial cells and several solid tumors[85-87].

Two main techniques can be used to functionalize the Au NCs with specific molecules. An efficient approach involves directly synthesizing Au NCs with the molecule of interest usually with a terminal thiol group that could bind to the metal surface[8, 9]. A second approach is based on the post-functionalization of Au NCs. Click chemistry[15] and succinimidyl ester[84, 88, 89] reaction have been used to covalently bind molecules of interest to the ligand stabilizing the Au NCs[15, 78, 82, 86], or ligand exchange could be used if the molecule of interest has a thiol group[89].

3 Physico-chemical parameters affecting the biodistribution of Au NCs

C. Zhou *et al*.[90] studied the biodistribution of AuSG with NIR emission. The highest uptake of the AuSG in the kidney (21% of **injected dose per gram of tissue, ID/g**) was obtained at 5 min **pi (post injection)** and decreased almost by 3 folds (7.5 ID/g) after urinary excretion. These observations were consistent with their short circulation time in blood (**half-life, $t_{1/2\alpha}$** ~5 min) and indicated that AuSG were mainly eliminated via the urinary system. The accumulation of AuSG in the liver and spleen was lower than that in the kidney (respectively 4 and 2.4% ID/g) and remained constant over time. After 48 h, more than 50% of the injected AuSG were eliminated.

We obtained comparable results with AuZw, which presented a short blood circulation time (**$t_{1/2\alpha}$** ~6 min)[91]. Using **laser-induced breakdown spectroscopy (LIBS)**, we detected a strong Au signal in the medulla of the kidney 30 min pi that was almost undetectable at 1 h.(**Figure 3a**) In contrast, a low but constant Au signal was observed in the liver and spleen during 24 h.**(Figure 3b and c, respectively)** These results were confirmed *ex vivo* by fluorescence and inductively coupled plasma mass spectrometry measurements.

These two studies demonstrated that ultra-small size Au NCs have a very rapid renal clearance, but it is important to better understand the different physicochemical parameters that may **affect the kinetics and completeness of this renal elimination.**

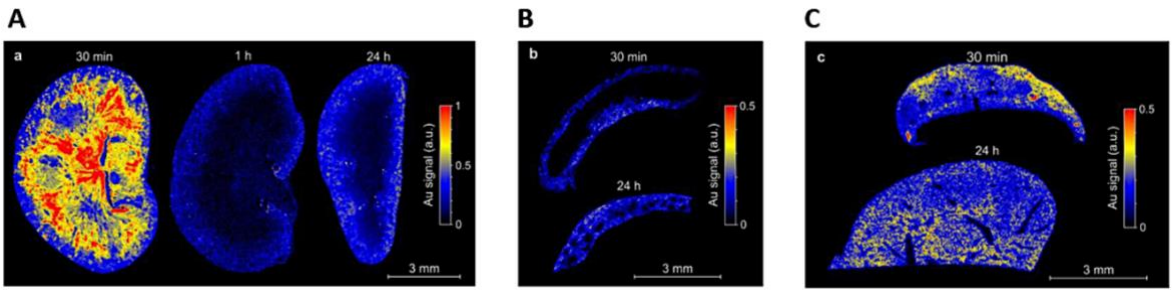

Figure 3. After the intravenous injection of $AuZwMe_2$ (600μM; 200 μL) into NMRI (Naval Medical Research Institute) nude mice, LIBS detection was carried out for:

(A) kidney slices 30 min, 1 h, and 24 h pi

(B) spleen slices 30 min and 24 h

(C) liver slices 30 min and 24 h

Reproduced from Ref [50] *with permission from The Royal Society of Chemistry publishing group.*

3.1 Length of the ligand

Due to the high surface reactivity of NCs, small changes in the ligand have huge impacts on their biodistribution. For example, the liver-to-blood and the kidney-to-blood ratios are decreased 22 and 1.9 times, respectively, when a glycine moiety is added to a cysteine ligand[21].

X.D. Zhang *et al.*[92] synthesized Au NCs with the same core size, but stabilized by different ligands such as SG or BSA. AuSG showed a very efficient renal clearance with 36% of the NCs excreted into the urine 24 h pi and only 6% were remaining in the mouse 28 days pi. In contrast, more than 95% of AuBSA were retained 28 days pi, with elevated concentrations in the liver and spleen (**Figure 4A**). This difference in terms of pharmacokinetics and biodistribution was attributed to the size of the ligand that changed the HD of the Au NCs. Indeed, the AuSG with its HD of 2 nm could be taken up by the kidney, but not the 7 nm of AuBSA[34, 93].

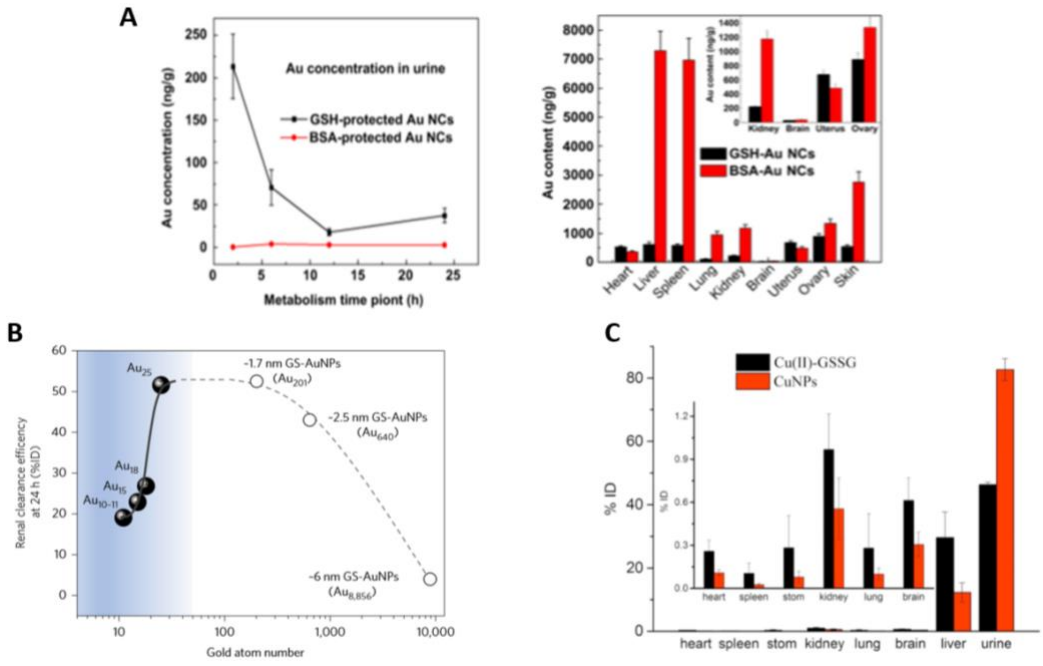

Figure 4.

(A) Renal elimination and biodistribution in mice intravenously injected (7 550 µg/kg, 151 µg/mL) with AuSG and AuBSA NCs : renal elimination 24 h pi (top left) and biodistribution in the main organs 28 days pi (top right). AuBSA NCs have 10 times higher distribution in the liver and spleen than AuSG NCs.

(B) Effect of the sub-nanometer size of the NCs in their renal elimination. Renal elimination efficiencies of different sizes of Au NCs, intravenously injected (~100 µM, 100 µL) in BALB/c mice, versus the number of gold atoms at 24 h pi. The renal elimination increased with the

number of gold atoms up to 25 ($Au_{25}SG_{18}$) and reached a plateau followed by a diminution for larger sizes.

(C) Biodistribution in the main organs 24 h after intravenous injections of Cu(II)-GSSG complexes (300 µL, 0.33 mg/mL) or luminescent CuSG NCs (300 uL, 0.83 mg/mL) in BALB/c mice (N=6).

Reproduced with permission from Elsevier for (A) Ref. [51]*, Springer Nature for (B) Ref.* [18c] *and American Chemical Society for (C) Ref.* [2e].

3.2 Size of the metal core

AuSG NPs with increasing metallic core sizes, leading to an increase in their HD (2, 6, and 13 nm) were administered intravenously[94] and, as could be expected, the results indicated that the larger the size, the stronger the liver uptake and the lower the kidney elimination**.** After one day pi, 50% of the **injected dose (ID)** of 2-nm large AuSG was eliminated in the urine, while only 4% or 0.5% ID for the 6- or 13-nm ones was observed. On the other hand, 3.7% ID, 27.1% ID, and 40.5% ID were respectively blocked in the liver. This tendency was also confirmed in a study that compared the clearance efficiency of 3.4- and 18.4-nm large Au NPs stabilized by SG[95]. However, a reverse size dependency has been observed recently when a sub-nanometer size was reached. $Au_{25}SG_{18}$ were filtered faster than $Au_{18}SG_{14}$ or $Au_{10\text{-}11}SG_{10\text{-}11}$[46]. (**Figure 4B**)

Accordingly, biodegradable NCs that dissociate into small fragments should also be cleared from the body. CuSG are 2 nm large NCs that gradually degrade in Cu(II)-SG and disulfide (Cu(II)-GSSG) under physiological conditions[6]. Surprisingly, 90% of the Cu collected in the urine 2 h pi was still in the form of CuSG, while 60% of Cu in the liver was in the form of Cu(II)-GSSG-complexes bound to serum proteins. Indeed, CuSG had a higher resistance to serum protein adsorption than Cu(II)-GSSG. This explains why these NCs were quickly eliminated and less accumulated in the liver than the degradation product. (**Figure 4C**)

3.3 Protein corona formation

Proteins can be adsorbed onto the surface of NPs forming the protein corona[93, 96]. The protein coating is a dynamic system with competition between different proteins until an equilibrium is reached. The first layer of proteins is rapidly adsorbed onto the surface of the particles to form the soft corona. In the second time, proteins that have a stronger affinity with the surface of the particles slowly remove the first layer of proteins to generate a stable layer: the hard corona. This means that the composition and thickness of the protein corona evolve with time[97]. The affinity and exchange rate of the protein

corona depend on the size, charge, composition, and shape of the NPs, the incubation conditions (temperature, concentration, and time), the type of proteins, and their stability[96, 97].

The formation of this protein layer will have an impact on cell internalization, bio-distribution, and toxicity of the NPs[98, 99], and NCs[100].

Concerning NCs, it was established that incubation of Au NCs with an increasing concentration of human serum albumin (HSA) improved their fluorescence intensity by 6 at high protein concentrations (3 μM)[101]. This was probably due to the adsorption of proteins that decreased the non-radiative recombination by forming a rigid protection layer or inducing new metal–ligands interactions.

The surface charge strongly affects the amount and composition of the protein corona[88]. Indeed, **negative** NCs interact preferentially with Apolipoprotein (Pi>5.5), whereas **positive** NCs prefer albumin (Pi <5.5), and as a result, positive NCs accumulate in the spleen, lung, heart, and kidney, while negatively charged NCs will rather end up in the liver and testis[88].

Neutral surfaces obtained with PEGylated ligands or with zwitterionic molecules (SG or BSA), are not binding proteins. However, the non-fouling properties observed with zwitterionic systems are **pH and particle curvature dependent**[14, 95, 102].

3.4 Density

Increasing the density of a NC will augment its interaction with the surface of the blood vessels. NCs stabilized by SG but with different metal cores (Au, Ag, and Au/Ag alloy) were synthesized[103]. As compared to high density AuSG, the low-density AgSG presented low affinities for the blood vessels, faster clearance, and shorter retention time.

3.5 Electrical charge

The charge of the NCs also determines the affinity of the NCs for the blood vessels. AuSG functionalized with ethanediamine or ethanedioic acid to generate positively and negatively charged surfaces were more slowly excreted than neutral NCs over a 90-day period[88]. Just 24 h after intraperitoneal administration, the amount of positively charged NCs in the kidney was two times higher than those of neutral NCs. Various studies had demonstrated that, after glomerular filtration, positively charged compounds bind through their cationic sites to megalin receptors overexpressed on negatively charged proximal tubule epithelial cells[50, 51, 104]. This re-absorption phenomenon could explain that small positively charged compounds were slowly excreted by the kidney.

3.6 Influence of the concentration of Au NCs injected

Finally, the concentration of the injected Au NCsalso influences its transport by the blood flow[105]. An interesting two-compartment kidney elimination process was observed for AuSG intravenously injected into mice at nine different concentrations (from 0.15 to 1 059 mg/kg). At low concentrations (<15 mg/kg), kidney elimination was constant at 35% ID. Then, the renal elimination linearly increased with the concentration of NCs. One explanation is that, for small doses, the AuSG could easily cross the blood vessel wall and enter the extravascular space. The reduction in their blood concentration slows down the renal process. At higher concentrations, the Au NCs are strictly confined to the blood vessels, more rapidly transported by the blood flow, and more efficiently eliminated through the kidney.

4 Tumor targeting of Au NCs

If the renal clearance of the NCs is reckoned as highly relevant to reduce their toxicity, these species should still have enough time to circulate in the body in order to accumulate passively and/or specifically in the tumor microenvironment. The growth of a tumor generally induces the formation of new blood vessels with pore sizes between 300 and 1200 nm and a perturbation of the lymphatic drainage. This allows NPs accumulation in cancer tissues at higher concentrations and for a longer time than in normal tissues. This phenomenon is called Enhanced Permeability and Retention (EPR) effect. Maeda *et al.*[106] were one of the first groups who studied the EPR effect in 1986. They discovered that NPs with a size larger than the KFT can circulate in the blood at high concentrations and for longer times (at least 6 h) to allow a passive uptake.

4.1 Passive accumulation of renal-clearable Au NCs by the EPR effect

Au NCs combine a high renal clearance with surprisingly elevated passive uptake in MCF-7 tumors[30]. As can be seen in **Figure 5A**, AuSG and IRDye 800CW present an rapid whole-body distribution and a maximum tumor accumulation 40 min pi. However, 24 h pi, the concentration of NCs in the tumor was 10 times higher than that of IRDye 800CW.(**Figure 5B**) This augmented EPR effect probably occurred because AuSG have a longer blood elimination half-life ($t_{1/2\beta}$) than IRDye.(**Figure 5C**)

Compared to larger Au NPs that are not cleared by the kidneys, AuSG present a two times higher tumor accumulation. This could be attributed to the 10 times lower accumulation of AuSG in the RES compared with Au NPs, which also maintained the highest NC concentration in the blood during the

first hours. This implies that NCs escaping RES uptake and remaining long enough in circulation in the blood stream will have a better chance to accumulate in tumors via the EPR effect.

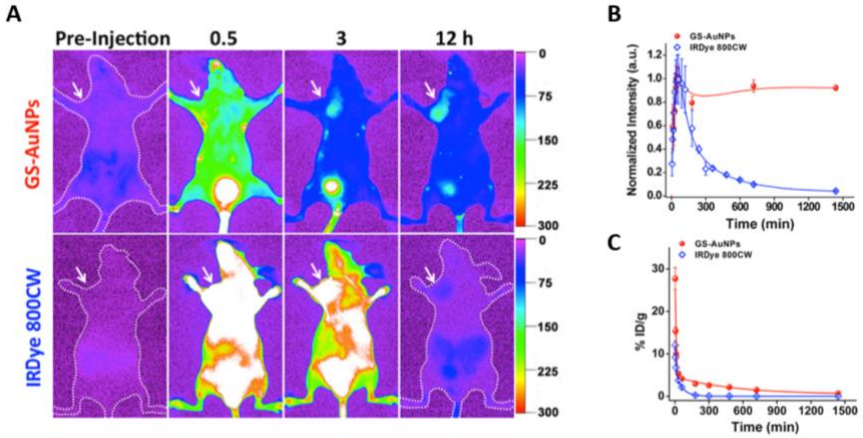

Figure 5. Tumor uptake and renal elimination in mice intravenously injected with AuSG NCs and IRDye 800CW

(A) In vivo NIR fluorescence images of MCF-7 tumor-bearing mice 0.5, 3, and 12 h after intravenous injection of AuSG NCs and IRDye 800CW (200 µL at 20 mg/mL and 10 µM, respectively). The tumor areas are indicated by arrows.

(B) MCF-7 tumor uptake of AuSG NCs and IRDye 800CW 24 h pi.

(C) Renal elimination of AuSG and IRDye 800CW, intravenously injected (200 µL at 7 mg/mL and 10 mM, respectively) during 24 h pi. The curves were fitted to biexponential function with R2 values of 0.9711 and 0.9838, respectively. The distribution half-life ($t_{1/2\alpha}$) are 5.4 +/- 1.2 and 6.3 +/- 2.5 min, respectively, and the $t_{1/2\beta}$ are 8.5 +/- 2.1 and 0.98 +/- 0.08h, respectively, for AuSG NCs and IRDye 800CW (n=3).

Reproduced from Ref. [9] *with permission from the American Chemical Society.*

4.1.1 Increasing the circulation time by reducing Au NC elimination by the kidney

Au NCs stabilized by SG or PEG ligands with close HD (3.3 and 5.5 nm, respectively) were tested[14] in order to study the impact of the ligand on renal elimination and tumor targeting. Both NCs were excreted to a similar extent at 24 h pi in the urine, but their kinetics of elimination were different. The fluorescence intensity of the bladder reached a maximum at 1 h for the AuSG, while it took 5 h for the AuPEG. It was thus not surprising that AuPEG showed a tumor accumulation in MCF-7 tumors three

times higher than that of AuSG at 12h pi. Similar results were obtained with $Au_{25}SG_{18}$ (~1.9 nm) and $AuZwMe_2$ (~2.36 nm)[33, 91] as well as when $Au_{25}SG_{18}$ were compared with smaller $Au_{10\text{-}11}SG_{10\text{-}11}$, $Au_{15}SG_{13}$, $Au_{18}SG_{14}$[46] (**Figure 6**). However, increasing the size of NCs with Au_{201} and Au_{640} had no impact on tumor uptake.

Overall, this confirms that increasing the circulation time of the NCs favors their passive uptake by the tumor.

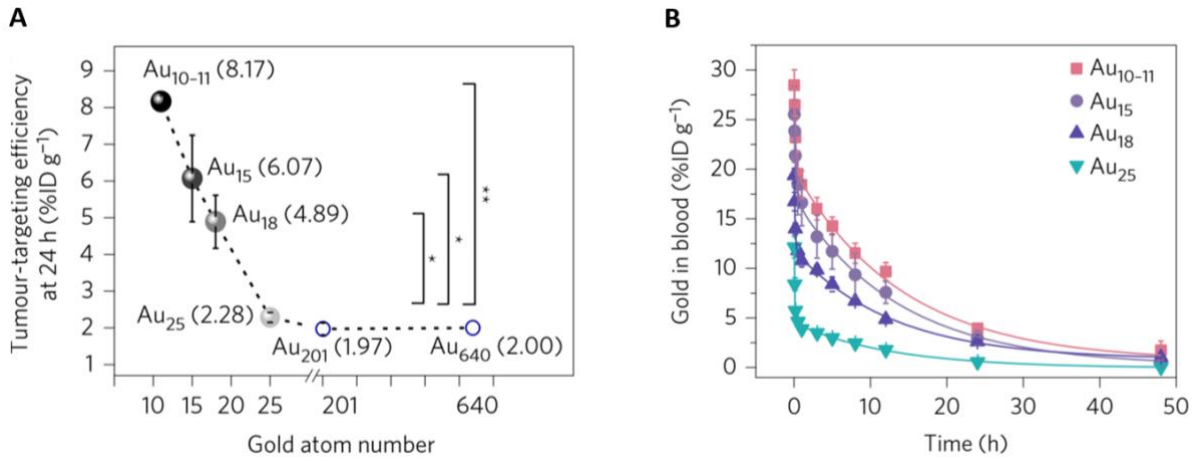

Figure 6. Effect of the subnanometer size of the NCs on tumor uptake

*(A) MCF-7 tumor accumulation efficiency of different-sized Au NCs versus the number of gold atoms at 24h p.i. For NCs smaller than $Au_{25}SG_{18}$ ($Au_{10\text{-}11}SG_{10\text{-}11}$, $Au_{15}SG_{13}$, $Au_{18}SG_{14}$), the tumor accumulation decreased with the increasing number of gold atoms. For NCs larger than $Au_{25}SG_{18}$. (Au_{201} and Au_{640}), tumor uptake was constant. *P<0.05, **P<0.005, Student's t-test.*

(B) Blood pharmacokinetics of $Au_{10\text{-}11}SG_{10\text{-}11}$, $Au_{15}SG_{13}$, $Au_{18}SG_{14}$, and $Au_{25}SG_{18}$ show two-compartment pharmacokinetics with different distributions and $t_{1/2\beta}$ between the NCs.

BALB/c mice (n=3) were intravenously injected (~100 µM, 100 µL).

Reproduced from Ref [18c] *with permission from Springer Nature publishing group.*

4.1.2 Increasing the cellular interaction

Neutral, positively, or negatively functionalized AuSG will not accumulate equally in tumors.[37] One day after intra-peritoneal administration, 149, 222, and 320 ng/g of Au NCs were measured in U14 tumors for neutral, positive, and negative NCs, respectively. The fact that charged Au NCs show higher tumor accumulation than neutral NCs could be explained by different phenomena. The negatively

charged cell membranes favor the adsorption of positively charged NCs, thus augmenting their binding to the cells and internalization[107]. For the negative ones, the enhancement of EPR effect is more likely due to the lower protein corona adsorption[108].

4.2 Active tumor targeting

The addition of a targeting agent, usually a small (bio)molecule that could specifically interact with receptors overexpressed at the surface of tumor cells is expected to augment the specific tumor accumulation. Cell surface proteins such as integrins, transferrin, and folate receptors (FRs) are commonly targeted because they are overexpressed in tumors[78-82, 85, 87, 109-111].

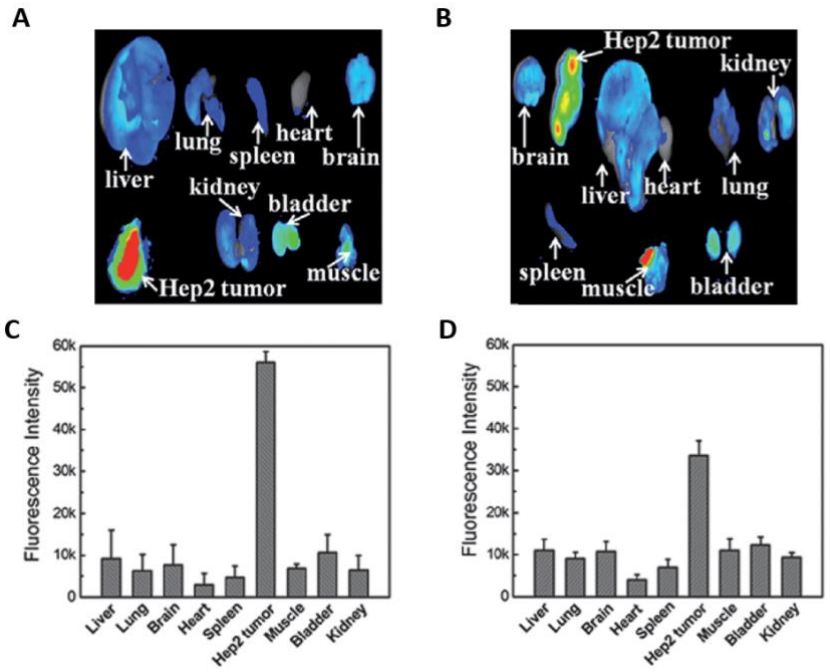

Figure 7. Ex vivo fluorescence images of the tumor and of the major organs in mice 7 h p.i of HA-AuBSA NCs (A) or free HA and AuBSA NCs (B) with the corresponding average fluorescence intensity analysis (C-D). The addition of the targeting ligand HA grafted onto the Au NCs surface improves the tumor uptake by two times.

Reproduced from Ref [44b] *with permission from The Royal Society of Chemistry publishing group.*

AuBSA functionalized with folic acid (FA)[49] provided a maximum tumor/normal tissue ratios (T/N) in mice with FR-positive HCT116 tumors two times higher than for negative A549 tumor. Functionalized the AuBSA with hyaluronic Acid (HA)[80] (**Figure 7)** or Luteinizing hormone-releasing hormone (LHRH)[83] allowed to increase the tumor accumulation by three compared to the AuBSA.

Grafting an RGD-containing peptide on AuBSA can improve the targeting of human glioblastoma U87MG tumors engrafted in mice[86]. U87MG cells are expressing integrin αvβ3, a cell surface receptor recognized by RGD. If, 1 h after the intravenous injection of AuBSA, the tumor was detected due to the EPR effect, the signal dramatically decreased after 2 h. In contrast, the NIR fluorescence of the RGD-Au in tumors was still visible after 24 h. Thus, functionalized Au NCs with a targeting molecule could improve the tumor accumulation of the Au NCs and prolong their retention time.

In another study, a dual targeting was tested. A cRGD peptide and a 26-base G-rich DNA oligonucleotide that functions as a nucleolin-binding aptamer (AS1411) were added to Au NCs to induce a dual targeting[38]. The nucleolin receptors are overexpressed on the cell membrane of most of the cancer cells. The tumor signal disappeared 8 h pi when naked Au NCs were used. In contrast, it was still detectable 48 h later when only one targeting molecule was added, confirming the interest of targeting to augment the retention time of the Au NCs in the tumor. If both ligands were co-presented by the Au NCs, the T/N fluorescence ratio was more elevated (7.2) than when the Au NCs were labeled with cRGD only (5.4).

If the addition of a targeting agent on the Au NCs surface favors higher and longer tumor accumulation[38, 81, 83, 84, 86], it also increases the size and changes the charge of the Au NCs, which could be at the expense of their renal elimination.

5 Au NCs: Promising theranostic agents

Au NCs are useful for multimodal cancer diagnosis and therapy.

5.1 Multimodal diagnostic applications

Many imaging techniques are used daily in hospitals for diagnosis, image-guided surgery, and follow-up of treatment efficacy. We will present only imaging techniques that were already tested with Au NCs in animal models.

5.1.1 Optical imaging

Optical imaging (OI) is a multiscale (from molecules to cells and up to the patient), noninvasive, and nonradiative technique[112] that facilitates real-time[59] *in vivo* monitoring with high sensitivity[113, 114] and temporal resolution to visualize dynamic processes[90].

However, OI presents also drawbacks and in particular suffer from a weak penetration of light in biological tissues, especially because hemoglobin absorbs light below 650 nm while water will absorb

wavelengths above 900 nm[112, 115]. In addition, in the visible range (± 400–700 nm), auto-fluorescence of some tissues (skin especially) leads to a high background noise that reduces the optical contrast. For all these reasons, it is particularly interesting to work in the NIR wavelengths range between 700 and 900 nm, called "transparent imaging window."[59, 112]

Au NCs, with their water solubility, biocompatibility, tunable PL from the UV to the NIR, and resistance to photobleaching are potentially good optical probes. In the earliest works, the low emission wavelength at 480 nm of Au NCs stabilized with histidine (His)[23] limited their use to superficial tissues or cell imaging. A hydrophilic indocyanine green fluorophore needed to be added to have an emission at 800 nm that can be followed *in vivo.* In the case of AuBSA, even though the 680 nm emission[80, 116, 117] enabled their detection under few millimeters of tissues, the conjugation with an indocyanine green fluorophore also permitted to shift the emission in the NIR and facilitated their detection[77]. As mentioned in the first part, several strategies exist to shift emission to higher wavelengths and to increase the QY of the NCs for improving their limit of detection. In the meantime, other NCs such as AuSG[14, 30] and AuPEG[14] with intrinsic NIR fluorescence were employed.

Seminal works by H. Dai[59, 115, 118] have demonstrated the benefit in terms of spatial and temporal resolutions to move from the NIR to a SWIR spectral window with the parallel development of new contrast agents and camera[59]. LA-sulfobetaine-capped Au NCs with relatively good fluorescence in the NIR/SWIR region (QY of 0.6% at 1000 nm and 3.8% at 900 nm) and broad emission were produced[58]. After their intravenous injection, images of the blood vessels were obtained with higher contrast and spatial resolution in the SWIR using a long-pass filter at 1250 nm than in the NIR.

Au NCs thus appeared as new promising SWIR **(Figure 8A)** and NIR **(Figure 8B)** contrast agents.

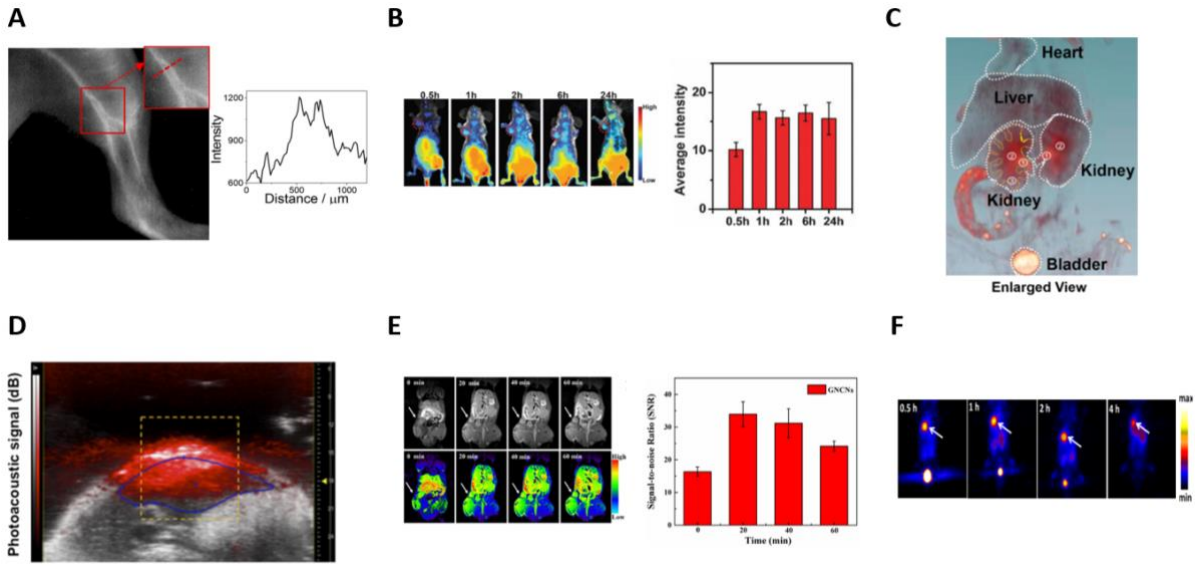

Figure 8.

(A) *Image of the left leg of a wild-type CS7BL/6 mouse taken using an InGaAs camera equipped with a 1250 LP filter after the intravenous injection of LA-sulfobetaine-capped Au NCs (0.5 mg of Au). Signal intensity across a line of interest drawn in the inset images showed the spatial resolution of the vessels.*

(B) *In vivo fluorescence images of a HeLa tumor-bearing nude mouse at different time points (30 min, 1 h, 2 h, 6 h, and 24 h) after intravenous injection of cRGD-Au NCs (200 μL, 8.0 mg/mL). Red circles indicate the tumor. Quantification of the signal intensity of the tumor side (n = 3).*

(C) *In vivo 3D CT images of the heart, liver, kidney, and bladder (excluding bone) in mice 2 h after intravenous injection of AuBSA NCs (200 μL, 9.5 mgAu/mL). The ureter, renal pelvis, and the major calyx are marked in orange and yellow dashed curves.*

(D) *Noninvasive in vivo photoacoustic imaging of the belly of a NMRI nude mouse, 3 h after intravenous injection of AuZw NCs (200μL, 600μM).*

(E) *In vivo T1-weighted MR images of A549 tumor in a BALB/c-nude mouse at different time points (20, 30, and 40 min) after intratumoral injection of Gd-AuSG NCs (50 μL, 0.11 M). White arrows indicate the position of the tumor. The graph represents the signal-to-noise ratio around the tumor. (n = 3)*

(F) *Representative PET images of coronal single slices of a orthotopic A549 lung tumor-bearing mouse at different time points (0.5, 1, 2, and 4 h), after intravenous injection of 6.7 MBq of [64Cu]CuNC@BSA-LHRH. White arrows indicate the position of the tumor.*

Reproduced with permission from American Chemical Society for (A) Ref. [29]*, (C) Ref.* [10a] *and (F) Ref.* [45] *; The Royal Society of Chemistry for (B) Ref.* [47a]*, AIP for (D) Ref.* [11] *and Elsevier for (E) Ref.* [79b].

5.1.2 X-ray CT

The X-ray CT is also a noninvasive technique[31] with a high 3D resolution that offers anatomical information, but suffers from low sensitivity[31, 114, 119, 120]. An additional contrast agent is often required to distinguish soft tissues[31, 120]. Iodine and gold are used as X-ray contrast agents[31, 120-122]; however, the short circulation time, nonspecific distribution, and potential renal toxicity of iodine limit its application. The idea is to find a compound slightly larger to increase the circulation time: Au NCs satisfies this criteria[94].

AuBSA were thus tested in mice, allowing an improved visualization of the structure of major organs (heart, liver, kidneys, bladder, and intestine) and a clear delineation of the calyces, pelvis, ureters, and

bladder (**Figure 8C**) making of AuBSA NC a promising candidate to study renal excretion[31]. Other NCs such as AuSG were also successfully tested[32].

Because the Au NCs are also fluorescent, they can be serve as bi-modal imaging agents[123]. X-ray CT images provide anatomical information, but can also be used to confirm the results obtained by optical imaging, such as tumor uptake[124] or renal elimination of AuSG[32, 35, 36, 94].

5.1.3 Photoacoustic

Au NCs have recently been employed in photoacoustic imaging[125] and OI [33] (**Figure 8D**). AuZw with different metal core sizes and ligand thicknesses were produced, in order to investigate the influence of the metal/ligand ratio on their optical and photoacoustic properties. When the amount of ligand increased, the shell became more rigid, which decreased the nonradiative loss due to vibrations of the ligand. This was associated with an increased fluorescence but decreased photoacoustic signal. However, by decreasing the quantity of ligand, the core of the NCs became larger. Upon illumination, the metallic core produced more heat, which generated more intense vibrations and ultimately improved the photoacoustic signal. Because of this opposite evolution in the signal, Au NCs should be carefully chosen, depending on the technique that will be required for the experiment.

5.1.4 Magnetic Resonance Imaging

Magnetic resonance Imaging (MRI) is a noninvasive technique[126] largely present in hospital and clinical settings based on the observation of water's protons contained in the organism when an external magnetic field is applied. This technique allows 3D reconstruction[114, 126] with high spatial resolution[120, 126], but suffers from low sensitivity[114, 120, 126]. Gadolinium (Gd^{3+}) is often used as a contrast agent for MRI detection[86, 127, 128].

The used of Au NCs decorated by Gd3+ ions compared to traditional Gd chelates (diethylenetriamine penta-acetic acid, DTPA) improved the performance of Gd as MRI contrast agent itself and o prolonged its detection time by three[128]. (**Figure 8E**) These Au NCs were still visible by by X-ray CT or optical imaging techniques which permit to visualize the organs, where MRI had a weak signal-to-noise ratio, making Gd-functionalized Au NCs promising tools for tri-modal imaging: MIR/X-ray CT/optical imaging.

5.1.5 Positron-Emitting Tomography

The last noninvasive imaging method described with Au NCs is positron-enhanced tomography (PET). PET has the highest detection sensitivity in human[39, 129] but a poor spatial resolution[114].

^{64}Cu, a well-known β^+ radioisotope, is generally complexed with bifunctional chelates, such as DOTA (1,4,7,10-tetraazacyclododecane-1,4,7,10tetraacetic acid) and TETA (1,4,8,11-tetraazacyclododecane1,4,8,11-tetraacetic acid). However, these complexes suffer from low stability, and the released copper ions will be complexed with proteins to be finally stored in the liver. This could induce toxic effects[83].

The direct incorporation of ^{64}Cu in NCs may exceed these limitations and the ligand shell could favor the radiolabeling stability. (**Figure 8F**) These NCs keep their initial properties, which means renal excretion and the ability to escape the RES[6, 83].

For example, CuSG NCs are progressively degraded into Cu(II)-GSSG[6]. Due to their interaction with serum proteins, they were then retained in the liver. After intravenous injection in mice, CuSG or Cu(II)-GSSG showed $t_{1/2\beta}$ of 3.2 and 4.9 h, respectively. The successful addition of ^{64}Cu, with its half-time of decay of 12.7 h, helped to follow the elimination of CuSG with precision. Indeed, the high signal into the kidney and the bladder just 1.5 min pi confirmed the fast renal elimination of [^{64}Cu]CuSG. The signal in the bladder still visible 4 h pi attested the constant elimination of the NCs from the body. Finally, at 4 h pi, the signal detected in the liver confirmed the dissociation of CuSG into Cu(II)-GSSG complexes. Radioactive NCs can thus be used for dual imaging. PET offers more sensitive and quantitative follow-up, which will come in addition to the benefits of optical imaging[83, 130].

5.2 Therapy

In addition to their interest for diagnostics, Au NCs can be used as therapeutic agents and delivery systems.

5.2.1 Radiotherapy

Gold can serve as a radiosensitizer[34-36] if it is formulated in order to be biocompatible, to have an efficient renal clearance and a good tumor accumulation capability.

Zhang *et al.* [35]first studied the potential of a $Au_{10-12}SG_{10-12.}$ or of a saline solution after intraperitoneal administration (0.2 mL, 3mM) in nude mice engrafted with a human cervical U14 tumor. When the tumor uptake reached a maximum (24 pi), the mice were either irradiated (under ^{137}Cs gamma radiation of 3 600 Ci at 5 Gy) or not. Regarding the controls, no decrease in tumor size was observed in mice treated with the Au NCs only over a period of 23 days. In contrast, the tumor volume decreased by 8% upon irradiation and 65% with the combination of Au NCs plus irradiation.

The same experiment was carried out with $Au_{29–43}SG_{27–37}$[36]. Compared with the control group, tumor volume in mice treated with radiation only and mice treated with both $Au_{29–43}SG_{27–37}$ and radiation decreased by 10% and 76%, respectively. No effects were observed in mice injected only with Au NCs. (**Figure 9A**) In both cases, Au NCs thus generated a toxic effect only if they were irradiated. Similar results were obtained with AuBSA[34].

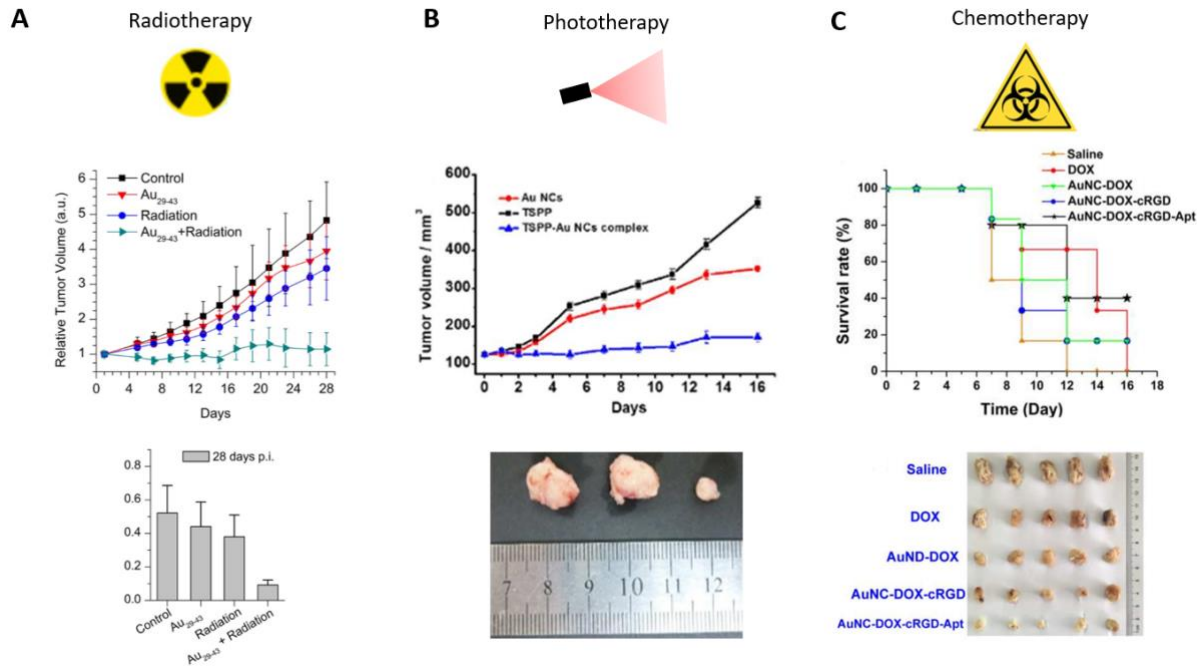

Figure 9.

(A) Time-course studies of the U14 tumor volumes until 28 days pi (top) and measurement of the U14 tumor weights at 28 days pi (bottom) of mice intraperitoneally injected with saline solution (control) or with $Au_{29–43}SG_{27–37}$ *(5.9 mgAu/kg of body), nude mice treated with radiation only (under* ^{137}Cs *gamma radiation of 3 600 Ci at 5 Gy, 24h pi), and nude mice injected with* $Au_{29–43}SG_{27–37}$ *followed by irradiation.(n = 8)*

(B) Time-course studies of U87 tumor volumes until 16 days pi (top) of mice intraperitoneally injected with Au NCs (0.1 mL, 5mM), TSPP (0.1 mL, 0.1 mM) and TSPP-Au NCs (equivalent 0.1 mL, 0.1 mM TSPP)(n = 3) and corresponding images isolated from tumor-bearing mice after 16 days of treatment (Au NCs, TSPP and TSPP-Au NCs from left to right, bottom)

(C) *Survival rate curves of U87MG tumor-bearing mice intravenously injected with free DOX, DOX-Au NCs, cRGD-DOX-Au NCs, and Apt-cRGD-DOX-Au NCs (all at 5.0 µg* kg^{-1} *equivalent DOX) and corresponding images isolated from tumor-bearing mice after 14 days of treatment (bottom)*

Reproduced from Ref [12], [71] *and* [13b] *with permission from Scientific Reports, The Royal Society of Chemistry and Elsevier publishing group.*

5.2.2 Phototherapy

The second well-developed approach in cancer treatment is phototherapy, divided in **photo-dynamic therapy (PDT)** and **photothermal therapy (PTT)** but the potential of Au NCs as PTT agents in mice has not been proven yet.

Concerning PDT, $Au_{25}SG_{18}$ can generate singlet oxygen species under 650 and 808 nm irradiation in solution[131] but most of the current studies are using Au NCs combined with photosensitizer molecules such as chlorine6 (Ce6)[37, 39, 132, 133] or porphyrin derivatives[37, 116].

Most of the PDT compounds are presenting unwanted cutaneous photosensitivity, and inadequate selectivity that can be ameliorated when combined with NCs. A four-time decrease in the size of C6 tumors was obtained 8 days after the intravenous injection of Au NCs grafted with protoporphyrin IX, followed 3 h later by laser treatment (532 nm, 15 min, 1.5W/cm^2)[37] compared to the control treated with radiation only. As well, U87 tumor growth can be stopped, after intratumoral injection of Au NCs conjugated with TSPP (meso-tetra(4-sulfonatophenyl)porphine dihydrochloride), a photosensitizer, in U87 tumors, and light excitation during 30 min per day with an IR light indicating that Au NCs can enhance the PDT effect of the photosensitizer alone[116]. (**Figure 9B**)

In order to study whether this synergistic effect could be generalized, C. Zhang *et al.*[39] intravenously injected Ce6-$Au_{25}SG_{18}$, free Ce6, or PBS into mice with human gastric MGC-803 tumors of 150 mm^3. The tumors were illuminated (633 nm, 10 min, 100 mW/cm^2) 8 h and 24 h later. After 21 days, the volumes of the tumors for the mice injected with PBS, Ce6, and Ce6-$Au_{25}SG_{18}$ without laser treatment were similar and close to 1 200 mm^3. However, the tumor growth slowed down and reached a volume around 650 mm^3 or 350 mm^3, in mice injected with free Ce6 or Ce6-$Au_{25}SG_{18}$ followed by illumination. This thus confirmed that Au NCs can enhance the radiotherapeutic activity of a co-injected radiosensitizer.

Based on this observation, it appeared interesting to generate a core–shell structure using silica[132] or liposomes[133] to increase the amount of Ce6 in contact with the Au NCs. The compounds were intravenously injected into mice with melanoma MDA-MB-435 or breast MDA-MB-361 tumors for compounds with silica or liposome shell, respectively. The tumors were irradiated for 10 min using laser (671 nm, 100 mW/cm^2) for the silica and 3 times every 3 days for 25 min (660 nm, 150 mW/cm^2) for the liposomes. In both tumor models, regarding the control, the injection of free Ce6 slowed down the growth of the tumors almost 2 times, while the core–shell structure composed of Ce6 and Au NCs totally inhibited the growth of the tumors. These studies confirmed that Au NCs can enhance the effect of the Ce6 radiosensitizer even after encapsulation in silica or liposomes.

5.2.3 Chemotherapy

Au NCs can also be used for drug delivery, as demonstrated with the delivery of doxorubicin (DOX), a DNA-intercalating agent[38]. After repeated intravenous administration every 48 h for 2 weeks, mice with U87MG tumors presented reduced tumor growth with increased necrosis as compared to controls (**Figure 9C**).

More complex systems combining multimodal imaging and therapeutic compounds were generated[132] combining Au NCs functionalized with Ce6 carbon dots. These theranostic agents were usable for fluorescence, MRI and PDT cancer treatment.

To conclude, Au NCs are promising multimodal imaging probes. Due to their intrinsic properties, toxic effects can be generated in the microenvironment of the tumors upon activation by an external stimulus like X-ray radiation or illumination, with reduced damages to healthy tissues. They can be used as therapeutic compounds alone or to enhance the effects of sensitizer agents.

The multimodal properties of the Au NCs make these theranostic agents highly promising in oncology.

5.2.4 Optical-guided surgery

Biocompatible zwitterionic or pegylated ligands containing Au NCs present augmented optical properties and plasma half-life that can improve their passive accumulation in an orthotopic animal model of Head and Neck Squamous Cell Carcinoma (HNSCC). This can serve to detect the presence of tumors in the mouth using non-invasive optical imaging, and can be used intra-operatively by surgeons to perform optical-guided surgery with improved survival rates as compared to standard surgery. Indeed, the presence of fluorescent-Au NCs labeling tumor margins allows the surgeon to better remove all tumor infiltrated surrounding tissues that are not visible by naked eyes, thus reducing the appearance of local relapse[76].

6 Conclusions and perspectives

In this review, we described recent works performed on metal NCs, mainly gold, for *in vivo* applications. Progress in synthesis methods has enabled the development of effective strategies to produce photoluminescent atomically precise NCs in large scales, with high purity and different functional groups.

The unique physicochemical properties and good biocompatibility of metal NCs have facilitated their use in biomedical applications. The PL and metallic composition of NCs allow their use as optical, X-ray probes, or radiosensitizer. By integrating Au NCs with other imaging or therapeutic agents, complex

systems could be achieved. These combinations result in powerful image-guided therapy that take advantage of each technique. Finally, their fast-renal elimination decreases their nonspecific accumulation in different organs, and thus, their toxicity.

Different parameters such as size, length, and charge of the ligands or density affect the formation of the protein corona, optical properties, biodistribution, targeting potential, renal elimination, tumor uptake, and biodegradability of metal NCs. Each of these parameters must be carefully addressed when designing NCs for specific biomedical applications and their possible clinical translation.

Au NCs have already been applied *in vivo* on mice and monkeys[105]. They have shown promising results as theranostic agents, even in parts of the body difficult to access. NCs are not limited to cancer treatments and can be used for diagnosis of other diseases such as renal dysfunctions[31, 134, 135], and Alzheimer's disease[136, 137].

However, some of their properties such as their tumor accumulation and retention or their luminescent properties in the NIR and SWIR for *in vivo* imaging still need to be improved. Further studies are necessary to confirm their radio and photosensitizing effects and more broadly, to get a deeper understanding of the relationships among structure, stability, and luminescence of Au NCs.

Precise and early diagnosis of the tumors and the development of targeted therapies are two major lines of research in oncology. In this context, we believe that photoluminescent Au NCs are promising candidates. Their biomedical potentials will go beyond cancer research and toward a wide range of (biomedical) applications (such as fluorophore for fluorescence resonance energy transfer applications[138, 139], biosensors, and optoelectronics).

7 Acknowledgement

XLG and EP would like to thank Cancéropôle Lyon Auvergne Rhône-Alpes (CLARA), Plan Cancer (C18038CS) and ARC (R17157CC) for their financial support. All authors declare that they have no financial/commercial Conflict of Interest.

8 References

1. R. Jin, C. Zeng, M. Zhou and Y. Chen, *Chemical Reviews*, 2016, **116**, 10346-10413.
2. J. Wang, J. Ye, H. Jiang, S. Gao, W. Ge, Y. Chen, C. Liu, C. Amatore and X. Wang, *RSC Advances*, 2014, **4**, 37790.
3. S. Gao, D. Chen, Q. Li, J. Ye, H. Jiang, C. Amatore and X. Wang, *Scientific Reports*, 2015, **4**.
4. D. Chen, C. Zhao, J. Ye, Q. Li, X. Liu, M. Su, H. Jiang, C. Amatore, M. Selke and X. Wang, *ACS Applied Materials & Interfaces*, 2015, **7**, 18163-18169.
5. C. Zhao, L. Lai, F. U. Rehman, C. Qian, G. Teng, H. Jiang and X. Wang, *RSC Adv.*, 2016, **6**, 110525-110534.
6. S. Yang, S. Sun, C. Zhou, G. Hao, J. Liu, S. Ramezani, M. Yu, X. Sun and J. Zheng, *Bioconjugate Chemistry*, 2015, **26**, 511-519.
7. C. J. Ackerson, P. D. Jadzinsky and R. D. Kornberg, *Journal of the American Chemical Society*, 2005, **127**, 6550-6551.
8. F. Aldeek, M. A. H. Muhammed, G. Palui, N. Zhan and H. Mattoussi, *ACS Nano*, 2013, **7**, 2509-2521.
9. X. Yuan, B. Zhang, Z. Luo, Q. Yao, D. T. Leong, N. Yan and J. Xie, *Angewandte Chemie International Edition*, 2014, **53**, 4623-4627.
10. H.-H. Wang, C.-A. J. Lin, C.-H. Lee, Y.-C. Lin, Y.-M. Tseng, C.-L. Hsieh, C.-H. Chen, C.-H. Tsai, C.-T. Hsieh, J.-L. Shen, W.-H. Chan, W. H. Chang and H.-I. Yeh, *ACS Nano*, 2011, **5**, 4337-4344.
11. L. Shang, N. Azadfar, F. Stockmar, W. Send, V. Trouillet, M. Bruns, D. Gerthsen and G. U. Nienhaus, *Small*, 2011, **7**, 2614-2620.
12. E. Porret, L. Sancey, A. Martín-Serrano, M. I. Montañez, R. Seeman, A. Yahia-Ammar, H. Okuno, F. Gomez, A. Ariza, N. Hildebrandt, J.-B. Fleury, J.-L. Coll and X. Le Guével, *Chemistry of Materials*, 2017, **29**, 7497-7506.
13. T. D. Fernández, J. R. Pearson, M. P. Leal, M. J. Torres, M. Blanca, C. Mayorga and X. Le Guével, *Biomaterials*, 2015, **43**, 1-12.
14. J. Liu, M. Yu, X. Ning, C. Zhou, S. Yang and J. Zheng, *Angewandte Chemie International Edition*, 2013, **52**, 12572-12576.
15. E. Oh, F. K. Fatemi, M. Currie, J. B. Delehanty, T. Pons, A. Fragola, S. Lévêque-Fort, R. Goswami, K. Susumu, A. L. Huston and I. L. Medintz, *Particle & Particle Systems Characterization*, 2013, **30**, 453-466.
16. H. Duan and S. Nie, *Journal of the American Chemical Society*, 2007, **129**, 2412-2413.
17. J. Zheng, C. Zhang and R. M. Dickson, *Physical Review Letters*, 2004, **93**.
18. F. Qu, N. B. Li and H. Q. Luo, *Analytical Chemistry*, 2012, **84**, 10373-10379.
19. J. T. Petty, J. Zheng, N. V. Hud and R. M. Dickson, *Journal of the American Chemical Society*, 2004, **126**, 5207-5212.
20. G. Liu, Y. Shao, K. Ma, Q. Cui, F. Wu and S. Xu, *Gold Bulletin*, 2012, **45**, 69-74.
21. X. Ning, C. Peng, E. S. Li, J. Xu, R. D. Vinluan, M. Yu and J. Zheng, *APL Materials*, 2017, **5**, 053406.
22. Y. Yu, Z. Luo, Y. Yu, J. Y. Lee and J. Xie, *ACS Nano*, 2012, **6**, 7920-7927.
23. H. Chen, B. Li, C. Wang, X. Zhang, Z. Cheng, X. Dai, R. Zhu and Y. Gu, *Nanotechnology*, 2013, **24**, 055704.
24. Y. Negishi, K. Nobusada and T. Tsukuda, *Journal of the American Chemical Society*, 2005, **127**, 5261-5270.
25. Q. Wen, Y. Gu, L.-J. Tang, R.-Q. Yu and J.-H. Jiang, *Analytical Chemistry*, 2013, **85**, 11681-11685.
26. R. D. Vinluan, J. Liu, C. Zhou, M. Yu, S. Yang, A. Kumar, S. Sun, A. Dean, X. Sun and J. Zheng, *ACS Applied Materials & Interfaces*, 2014, **6**, 11829-11833.
27. J. Xie, Y. Zheng and J. Y. Ying, *Journal of the American Chemical Society*, 2009, **131**, 888-889.
28. A. Baksi, P. L. Xavier, K. Chaudhari, N. Goswami, S. K. Pal and T. Pradeep, *Nanoscale*, 2013, **5**, 2009.
29. X. L. Guével, N. Daum and M. Schneider, *Nanotechnology*, 2011, **22**, 275103.
30. J. Liu, M. Yu, C. Zhou, S. Yang, X. Ning and J. Zheng, *Journal of the American Chemical Society*, 2013, **135**, 4978-4981.
31. Y. Wang, C. Xu, J. Zhai, F. Gao, R. Liu, L. Gao, Y. Zhao, Z. Chai and X. Gao, *Analytical Chemistry*, 2015, **87**, 343-345.
32. J. Xu, M. Yu, P. Carter, E. Hernandez, A. Dang, P. Kapur, J.-T. Hsieh and J. Zheng, *Angewandte Chemie International Edition*, 2017, **56**, 13356-13360.
33. D. Shen, M. Henry, V. Trouillet, C. Comby-Zerbino, F. Bertorelle, L. Sancey, R. Antoine, J.-L. Coll, V. Josserand and X. Le Guével, *APL Materials*, 2017, **5**, 053404.
34. X.-D. Zhang, J. Chen, Z. Luo, D. Wu, X. Shen, S.-S. Song, Y.-M. Sun, P.-X. Liu, J. Zhao, S. Huo, S. Fan, F. Fan, X.-J. Liang and J. Xie, *Advanced Healthcare Materials*, 2014, **3**, 133-141.
35. X.-D. Zhang, Z. Luo, J. Chen, X. Shen, S. Song, Y. Sun, S. Fan, F. Fan, D. T. Leong and J. Xie, *Advanced Materials*, 2014, **26**, 4565-4568.
36. X.-D. Zhang, Z. Luo, J. Chen, S. Song, X. Yuan, X. Shen, H. Wang, Y. Sun, K. Gao, L. Zhang, S. Fan, D. T. Leong, M. Guo and J. Xie, *Scientific Reports*, 2015, **5**.
37. L. V. Nair, S. S. Nazeer, R. S. Jayasree and A. Ajayaghosh, *ACS Nano*, 2015, **9**, 5825-5832.
38. D. Chen, B. Li, S. Cai, P. Wang, S. Peng, Y. Sheng, Y. He, Y. Gu and H. Chen, *Biomaterials*, 2016, **100**, 1-16.
39. C. Zhang, C. Li, Y. Liu, J. Zhang, C. Bao, S. Liang, Q. Wang, Y. Yang, H. Fu, K. Wang and D. Cui, *Advanced Functional Materials*, 2015, **25**, 1314-1325.
40. X.-R. Song, N. Goswami, H.-H. Yang and J. Xie, *The Analyst*, 2016, **141**, 3126-3140.
41. Y. Negishi, Y. Takasugi, S. Sato, H. Yao, K. Kimura and T. Tsukuda, *Journal of the American Chemical Society*, 2004, **126**, 6518-6519.
42. Y. Shichibu, Y. Negishi, H. Tsunoyama, M. Kanehara, T. Teranishi and T. Tsukuda, *Small*, 2007, **3**, 835-839.

43. M. A. Habeeb Muhammed and T. Pradeep, *Chemical Physics Letters*, 2007, **449**, 186-190.
44. R. Jin, H. Qian, Z. Wu, Y. Zhu, M. Zhu, A. Mohanty and N. Garg, *The Journal of Physical Chemistry Letters*, 2010, **1**, 2903-2910.
45. N. Goswami, Q. Yao, T. Chen and J. Xie, *Coordination Chemistry Reviews*, 2016, **329**, 1-15.
46. B. Du, X. Jiang, A. Das, Q. Zhou, M. Yu, R. Jin and J. Zheng, *Nature Nanotechnology*, 2017, **12**, 1096-1102.
47. N. Goswami, Q. Yao, Z. Luo, J. Li, T. Chen and J. Xie, *The Journal of Physical Chemistry Letters*, 2016, **7**, 962-975.
48. M. A. H. Muhammed, F. Aldeek, G. Palui, L. Trapiella-Alfonso and H. Mattoussi, *ACS Nano*, 2012, **6**, 8950-8961.
49. J. Zheng, C. Zhou, M. Yu and J. Liu, *Nanoscale*, 2012, **4**, 4073.
50. B. Du, M. Yu and J. Zheng, *Nature Reviews Materials*, 2018, **3**, 358-374.
51. M. Longmire, P. L. Choyke and H. Kobayashi, *Nanomedicine*, 2008, **3**, 703-717.
52. A. K. Iyer, G. Khaled, J. Fang and H. Maeda, *Drug Discovery Today*, 2006, **11**, 812-818.
53. E. Blanco, H. Shen and M. Ferrari, *Nature Biotechnology*, 2015, **33**, 941-951.
54. L. Yang, H. Kuang, W. Zhang, Z. P. Aguilar, H. Wei and H. Xu, *Scientific Reports*, 2017, **7**.
55. E. B. Ehlerding, F. Chen and W. Cai, *Advanced Science*, 2016, **3**, 1500223.
56. Y.-S. Chen, Y.-C. Hung, I. Liau and G. S. Huang, *Nanoscale Research Letters*, 2009, **4**, 858-864.
57. X. L. Guevel, O. Tagit, C. E. Rodríguez, V. Trouillet, M. Pernia Leal and N. Hildebrandt, *Nanoscale*, 2014, **6**, 8091-8099.
58. Y. Chen, D. M. Montana, H. Wei, J. M. Cordero, M. Schneider, X. Le Guével, O. Chen, O. T. Bruns and M. G. Bawendi, *Nano Letters*, 2017, **17**, 6330-6334.
59. G. Hong, A. L. Antaris and H. Dai, *Nature Biomedical Engineering*, 2017, **1**, 0010.
60. B. Santiago-González, C. Vázquez-Vázquez, M. C. Blanco-Varela, J. M. Gaspar Martinho, J. M. Ramallo-López, F. G. Requejo and M. A. López-Quintela, *Journal of Colloid and Interface Science*, 2015, **455**, 154-162.
61. Y.-C. Shiang, C.-C. Huang, W.-Y. Chen, P.-C. Chen and H.-T. Chang, *Journal of Materials Chemistry*, 2012, **22**, 12972.
62. S. Link, A. Beeby, S. FitzGerald, M. A. El-Sayed, T. G. Schaaff and R. L. Whetten, *The Journal of Physical Chemistry B*, 2002, **106**, 3410-3415.
63. A. Mooradian, *Physical Review Letters*, 1969, **22**, 185-187.
64. A. Ghosh, T. Udayabhaskararao and T. Pradeep, *The Journal of Physical Chemistry Letters*, 2012, **3**, 1997-2002.
65. Y. Yu, Z. Luo, D. M. Chevrier, D. T. Leong, P. Zhang, D.-e. Jiang and J. Xie, *Journal of the American Chemical Society*, 2014, **136**, 1246-1249.
66. S. Wang, X. Meng, A. Das, T. Li, Y. Song, T. Cao, X. Zhu, M. Zhu and R. Jin, *Angewandte Chemie International Edition*, 2014, **53**, 2376-2380.
67. X. Le Guével, V. Trouillet, C. Spies, K. Li, T. Laaksonen, D. Auerbach, G. Jung and M. Schneider, *Nanoscale*, 2012, **4**, 7624.
68. E. Oh, J. B. Delehanty, L. D. Field, A. J. Mäkinen, R. Goswami, A. L. Huston and I. L. Medintz, *Chemistry of Materials*, 2016, **28**, 8676-8688.
69. Z. Wu and R. Jin, *Nano Letters*, 2010, **10**, 2568-2573.
70. G. Wang, R. Guo, G. Kalyuzhny, J.-P. Choi and R. W. Murray, *The Journal of Physical Chemistry B*, 2006, **110**, 20282-20289.
71. K. Pyo, V. D. Thanthirige, K. Kwak, P. Pandurangan, G. Ramakrishna and D. Lee, *Journal of the American Chemical Society*, 2015, **137**, 8244-8250.
72. H.-H. Deng, X.-Q. Shi, F.-F. Wang, H.-P. Peng, A.-L. Liu, X.-H. Xia and W. Chen, *Chemistry of Materials*, 2017, **29**, 1362-1369.
73. Y. Hong, J. W. Y. Lam and B. Z. Tang, *Chemical Society Reviews*, 2011, **40**, 5361.
74. Z. Luo, X. Yuan, Y. Yu, Q. Zhang, D. T. Leong, J. Y. Lee and J. Xie, *Journal of the American Chemical Society*, 2012, **134**, 16662-16670.
75. A. Yahia-Ammar, D. Sierra, F. Mérola, N. Hildebrandt and X. Le Guével, *ACS Nano*, 2016, **10**, 2591-2599.
76. C. Colombé, X. Le Guével, A. Martin-Serrano, M. Henry, E. Porret, C. Comby-Zerbino, R. Antoine, I. Atallah, B. Busser, J.-L. Coll, C. A. Righini and L. Sancey, *Nanomedicine: Nanotechnology, Biology and Medicine*, 2019, **20**, 102011.
77. H. Chen, B. Li, X. Ren, S. Li, Y. Ma, S. Cui and Y. Gu, *Biomaterials*, 2012, **33**, 8461-8476.
78. H. Chen, S. Li, B. Li, X. Ren, S. Li, D. M. Mahounga, S. Cui, Y. Gu and S. Achilefu, *Nanoscale*, 2012, **4**, 6050.
79. K. Pyo, N. H. Ly, S. Y. Yoon, Y. Shen, S. Y. Choi, S. Y. Lee, S.-W. Joo and D. Lee, *Advanced Healthcare Materials*, 2017, DOI: 10.1002/adhm.201700203, 1700203.
80. P. Zhang, X. X. Yang, Y. Wang, N. W. Zhao, Z. H. Xiong and C. Z. Huang, *Nanoscale*, 2014, **6**, 2261.
81. D. Chen, Z. Luo, N. Li, J. Y. Lee, J. Xie and J. Lu, *Advanced Functional Materials*, 2013, **23**, 4324-4331.
82. Y. Wang, C. Dai and X.-P. Yan, *Chem. Commun.*, 2014, **50**, 14341-14344.
83. F. Gao, P. Cai, W. Yang, J. Xue, L. Gao, R. Liu, Y. Wang, Y. Zhao, X. He, L. Zhao, G. Huang, F. Wu, Y. Zhao, Z. Chai and X. Gao, *ACS Nano*, 2015, **9**, 4976-4986.
84. Y. Zhao, L. Detering, D. Sultan, M. L. Cooper, M. You, S. Cho, S. L. Meier, H. Luehmann, G. Sun, M. Rettig, F. Dehdashti, K. L. Wooley, J. F. DiPersio and Y. Liu, *ACS Nano*, 2016, **10**, 5959-5970.
85. X. Wang, H. He, Y. Wang, J. Wang, X. Sun, H. Xu, W. M. Nau, X. Zhang and F. Huang, *Chem. Commun.*, 2016, **52**, 9232-9235.
86. S.-K. Sun, L.-X. Dong, Y. Cao, H.-R. Sun and X.-P. Yan, *Analytical Chemistry*, 2013, **85**, 8436-8441.
87. S. Lucie, G. Elisabeth, F. Stéphanie, S. Guy, H. Amandine, A.-R. Corinne, B. Didier, S. Catherine, G. Alexeï, D. Pascal and C. Jean-Luc, *Molecular Therapy*, 2009, **17**, 837-843.

88. X. Zhang, J. Chen, J.-Y. Wang, H. Wang, X. Shen, Y.-M. Sun, G. Meili and J. Yang, *International Journal of Nanomedicine*, 2016, **Volume 11**, 3475-3485.
89. E. S. Shibu, M. A. H. Muhammed, T. Tsukuda and T. Pradeep, *The Journal of Physical Chemistry C*, 2008, **112**, 12168-12176.
90. C. Zhou, G. Hao, P. Thomas, J. Liu, M. Yu, S. Sun, O. K. Öz, X. Sun and J. Zheng, *Angewandte Chemie*, 2012, **124**, 10265-10269.
91. X. Le Guével, M. Henry, V. Motto-Ros, E. Longo, M. I. Montañez, F. Pelascini, O. de La Rochefoucauld, P. Zeitoun, J.-L. Coll, V. Josserand and L. Sancey, *Nanoscale*, 2018, **10**, 18657-18664.
92. X.-D. Zhang, D. Wu, X. Shen, P.-X. Liu, F.-Y. Fan and S.-J. Fan, *Biomaterials*, 2012, **33**, 4628-4638.
93. I. Lynch and K. A. Dawson, *Nano Today*, 2008, **3**, 40-47.
94. C. Zhou, M. Long, Y. Qin, X. Sun and J. Zheng, *Angewandte Chemie International Edition*, 2011, **50**, 3168-3172.
95. C. Peng, X. Gao, J. Xu, B. Du, X. Ning, S. Tang, R. M. Bachoo, M. Yu, W.-P. Ge and J. Zheng, *Nano Research*, 2017, **10**, 1366-1376.
96. C. D. Walkey and W. C. W. Chan, *Chem. Soc. Rev.*, 2012, **41**, 2780-2799.
97. P. d. Pino, B. Pelaz, Q. Zhang, P. Maffre, G. U. Nienhaus and W. J. Parak, *Mater. Horiz.*, 2014, **1**, 301-313.
98. P. Aggarwal, J. B. Hall, C. B. McLeland, M. A. Dobrovolskaia and S. E. McNeil, *Advanced Drug Delivery Reviews*, 2009, **61**, 428-437.
99. R. D. Vinluan and J. Zheng, *Nanomedicine*, 2015, **10**, 2781-2794.
100. L. Shang and G. U. Nienhaus, *The International Journal of Biochemistry & Cell Biology*, 2016, **75**, 175-179.
101. L. Shang, S. Brandholt, F. Stockmar, V. Trouillet, M. Bruns and G. U. Nienhaus, *Small*, 2012, **8**, 661-665.
102. D. F. Moyano, K. Saha, G. Prakash, B. Yan, H. Kong, M. Yazdani and V. M. Rotello, *ACS Nano*, 2014, **8**, 6748-6755.
103. S. Tang, C. Peng, J. Xu, B. Du, Q. Wang, R. D. Vinluan, M. Yu, M. J. Kim and J. Zheng, *Angewandte Chemie International Edition*, 2016, **55**, 16039-16043.
104. A. Briat, C. H. F. Wenk, M. Ahmadi, M. Claron, D. Boturyn, V. Josserand, P. Dumy, D. Fagret, J.-L. Coll, C. Ghezzi, L. Sancey and J.-P. Vuillez, *Cancer Science*, 2012, **103**, 1105-1110.
105. J. Xu, M. Yu, C. Peng, P. Carter, J. Tian, X. Ning, Q. Zhou, Q. Tu, G. Zhang, A. Dao, X. Jiang, P. Kapur, J.-T. Hsieh, X. Zhao, P. Liu and J. Zheng, *Angewandte Chemie*, 2018, **130**, 272-277.
106. J. Fang, H. Nakamura and H. Maeda, *Advanced Drug Delivery Reviews*, 2011, **63**, 136-151.
107. E. Koren and V. P. Torchilin, *Trends in Molecular Medicine*, 2012, **18**, 385-393.
108. F. Alexis, E. Pridgen, L. K. Molnar and O. C. Farokhzad, *Molecular Pharmaceutics*, 2008, **5**, 505-515.
109. Y. Wang, J.-T. Chen and X.-P. Yan, *Analytical Chemistry*, 2013, **85**, 2529-2535.
110. C. Sun, H. Yang, Y. Yuan, X. Tian, L. Wang, Y. Guo, L. Xu, J. Lei, N. Gao, G. J. Anderson, X.-J. Liang, C. Chen, Y. Zhao and G. Nie, *Journal of the American Chemical Society*, 2011, **133**, 8617-8624.
111. G. Liang, X. Jin, S. Zhang and D. Xing, *Biomaterials*, 2017, **144**, 95-104.
112. R. Weissleder, *Nature Biotechnology*, 2001, **19**, 316-317.
113. S. Wang, N. Li, W. Pan and B. Tang, *TrAC Trends in Analytical Chemistry*, 2012, **39**, 3-37.
114. S. Lee and X. Chen, *Molecular Imaging*, 2009, **8**, 7290.2009.00013.
115. G. Hong, S. Diao, J. Chang, A. L. Antaris, C. Chen, B. Zhang, S. Zhao, D. N. Atochin, P. L. Huang, K. I. Andreasson, C. J. Kuo and H. Dai, *Nature Photonics*, 2014, **8**, 723-730.
116. Y. Zhang, J. Li, H. Jiang, C. Zhao and X. Wang, *RSC Adv.*, 2016, **6**, 63331-63337.
117. X. Wu, X. He, K. Wang, C. Xie, B. Zhou and Z. Qing, *Nanoscale*, 2010, **2**, 2244.
118. G. Hong, J. C. Lee, J. T. Robinson, U. Raaz, L. Xie, N. F. Huang, J. P. Cooke and H. Dai, *Nature Medicine*, 2012, **18**, 1841-1846.
119. L. W. Goldman, *Journal of Nuclear Medicine Technology*, 2007, **35**, 115-128.
120. M. F. Kircher and J. K. Willmann, *Radiology*, 2012, **263**, 633-643.
121. J. T. Au, G. Craig, V. Longo, P. Zanzonico, M. Mason, Y. Fong and P. J. Allen, *American Journal of Roentgenology*, 2013, **200**, 1347-1351.
122. J. F. Hainfeld, D. N. Slatkin, T. M. Focella and H. M. Smilowitz, *The British Journal of Radiology*, 2006, **79**, 248-253.
123. A. Zhang, Y. Tu, S. Qin, Y. Li, J. Zhou, N. Chen, Q. Lu and B. Zhang, *Journal of Colloid and Interface Science*, 2012, **372**, 239-244.
124. C. Zhang, Z. Zhou, Q. Qian, G. Gao, C. Li, L. Feng, Q. Wang and D. Cui, *Journal of Materials Chemistry B*, 2013, **1**, 5045.
125. H. F. Zhang, K. Maslov, G. Stoica and L. V. Wang, *Nature Biotechnology*, 2006, **24**, 848-851.
126. J.-H. Lee, Y.-M. Huh, Y.-w. Jun, J.-w. Seo, J.-t. Jang, H.-T. Song, S. Kim, E.-J. Cho, H.-G. Yoon, J.-S. Suh and J. Cheon, *Nature Medicine*, 2007, **13**, 95-99.
127. G. Liang, D. Ye, X. Zhang, F. Dong, H. Chen, S. Zhang, J. Li, X. Shen and J. Kong, *Journal of Materials Chemistry B*, 2013, **1**, 3545.
128. W. Hou, F. Xia, G. Alfranca, H. Yan, X. Zhi, Y. Liu, C. Peng, C. Zhang, J. M. de la Fuente and D. Cui, *Biomaterials*, 2017, **120**, 103-114.
129. S. S. Gambhir, *Nature Reviews Cancer*, 2002, **2**, 683-693.
130. F. Chen, S. Goel, R. Hernandez, S. A. Graves, S. Shi, R. J. Nickles and W. Cai, *Small*, 2016, **12**, 2775-2782.
131. H. Kawasaki, S. Kumar, G. Li, C. Zeng, D. R. Kauffman, J. Yoshimoto, Y. Iwasaki and R. Jin, *Chemistry of Materials*, 2014, **26**, 2777-2788.

132. P. Huang, J. Lin, S. Wang, Z. Zhou, Z. Li, Z. Wang, C. Zhang, X. Yue, G. Niu, M. Yang, D. Cui and X. Chen, *Biomaterials*, 2013, **34**, 4643-4654.
133. F. Gao, W. Zheng, L. Gao, P. Cai, R. Liu, Y. Wang, Q. Yuan, Y. Zhao and X. Gao, *Advanced Healthcare Materials*, 2017, **6**, 1601453.
134. M. Zhou, C. Zeng, Y. Chen, S. Zhao, M. Y. Sfeir, M. Zhu and R. Jin, *Nature Communications*, 2016, **7**, 13240.
135. M. Yu, J. Zhou, B. Du, X. Ning, C. Authement, L. Gandee, P. Kapur, J.-T. Hsieh and J. Zheng, *Angewandte Chemie International Edition*, 2016, **55**, 2787-2791.
136. L. Lai, C. Zhao, X. Li, X. Liu, H. Jiang, M. Selke and X. Wang, *RSC Adv.*, 2016, **6**, 30081-30088.
137. L. Lai, X. Jiang, S. Han, C. Zhao, T. Du, F. U. Rehman, Y. Zheng, X. Li, X. Liu, H. Jiang and X. Wang, *Langmuir*, 2017, **33**, 9018-9024.
138. M. A. H. Muhammed, A. K. Shaw, S. K. Pal and T. Pradeep, *The Journal of Physical Chemistry C*, 2008, **112**, 14324-14330.
139. E. Oh, A. L. Huston, A. Shabaev, A. Efros, M. Currie, K. Susumu, K. Bussmann, R. Goswami, F. K. Fatemi and I. L. Medintz, *Scientific Reports*, 2016, **6**.